Conf-8708186--7

MICAP: A Program for Low Energy Neutron, Ion, and Gamma-ray Transport and One of Its Applications in Calorimeter Design: Hydrogen Knock-in as a Method for Achieving Compensation*

CONF-8708186--7

DE90 000568

T. A. Gabriel, J. O. Johnson
Engineering Physics and Mathematics Division
Oak Ridge National Laboratory
Oak Ridge, Tn 37831

J. Brau
Department of Physics
University of Tennessee
Knoxville, TN

Presented and published in the Proceedings of the Workshop on Detector Simulation for the SSC Argonne National Laboratory, August 24-28, 1987.

*Research sponsored by Office of High Energy and Nuclear Physics, U.S. Department of Energy under Contract no. DE-AC05-84OR21400 with Martin Marietta Energy Systems, Inc.

DISCLAIMER

MICAP: A PROGRAM FOR LOW ENERGY NEUTRON, ION, AND GAMMA-RAY TRANSPORT AND ONE OF ITS APPLICATIONS IN CALORIMETER DESIGN: HYDROGEN KNOCK-IN AS A METHOD FOR ACHIEVING COMPENSATION

T. A. Gabriel and J. O. Johnson
Oak Ridge National Laboratory, Oak Ridge, TN 37831, USA

J. Brau
Department of Physics, University of Tennessee, Knoxville, TN, USA

ABSTRACT

A new code system, MICAP, has been developed for the transport and production of low-energy (<20 MeV) neutrons, photons, and light and heavy ions. The results generated by this code system compare favorably with a wide variety of experimental data. Because of this success, MICAP can be used as a valuable tool in helping to analyze calorimeter systems. In particular, MICAP is used in this paper to determine the practicality of hydrogen knock-in as a method of achieving compensation in a uranium/silicon calorimeter, i.e., e/h = 1. The results indicate that compensation is probably possible but shower fluctuations may be increased.

1. INTRODUCTION

The use of silicon as the active medium in electromagnetic and hadronic calorimeters is gaining acceptance as a possible material of choice.[1,2] The advantages of silicon are many and include absolute gain for the sampling medium, gain adjustment and monitoring by radioactive sources, non-saturating readout (so sources give absolute energy scale), fast charge collection, fine lateral and longitudinal segmentation, etc. However, there are also several major disadvantages which include small sampling fraction (silicon strips are generally 0.04 cm thick), cost (silicon strips and associated electronics are relatively expensive), susceptibility to radiation damage, and insensitivity to low-energy neutron collisions, i.e., small amounts of energy transfer.

For many years it has been recognized that one limitation on hadronic calorimetry is due to the nuclear binding energy fluctuations and the resulting unequal response of a calorimeter to electromagnetic and nonelectromagnetic components of a hadronic shower. The unequal response can be measured by comparing the pulse height (e and h) of electromagnetic showers and hadronic showers. These two responses can be brought closer to

equality ($e/h \approx 1$) by using high Z radiators and taking advantage of the preferential deposition of the electromagnetic energy in the radiator.[3] In addition, by amplifying the nuclear break-up energy through the use of uranium radiators, the nonelectromagnetic response can be increased.[2] These two effects can bring the relative responses to a state of near equality. The nuclear amplification process relies on efficient detection in the sampling medium of low-energy neutrons, best accomplished by the use of hydrogenous materials (for example, scintillator).

Because of the insensitivity to low-energy neutrons, a calorimeter composed of only uranium and silicon will have an electron-to-hadron (e/h) pulse ratio greater than 1.0. To increase the hadronic signal such that $e/h \approx 1.0$, a more efficient detection of the low-energy neutrons must occur. The method most often suggested by the authors[3] and others[2,4] is to couple a hydrogenous medium to the active medium (silicon). Some of the recoil protons produced by MeV neutron collisions in the hydrogenous material should have sufficient range to reach the silicon thereby producing additional signal. Presented in this paper are a series of calculations carried out to obtain the amount of knock-in proton energy that can be obtained. It will be shown that the signal can be increased due to these knock-in protons, however, the amount of increase may not be sufficient to reduce the e/h ratio to ≈ 1.0 without an increase in shower fluctuation and therefore an increase in energy resolution.

To analyze hydrogen knock-in and low-energy neutron transport and gamma-ray production in general requires a very detailed analog Monte Carlo transport code. A second purpose of this paper is to describe MICAP,[5] a code system capable of analyzing in detail hydrogen knock-in. MICAP was developed because existing general purpose Monte Carlo code systems, i.e., MORSE,[6] MCNP,[7] and TRIPOLI[8] have all been written for neutral particle transport analysis. As such, these codes concentrate on the interactions affecting the neutrons and photons without regard to the charged products of the reaction; i.e., protons, deuterons, alpha particles, heavy ions, etc. Consequently, these codes do not model the details of charged particle production and do not transport the low energy charged particles essential to detector response analysis. MICAP as a stand-alone code or as part of the CALOR[9] system provides a new computational tool which eliminates most of the shortcomings of the methods currently being used to analyze

low-energy neutrons in calorimeter systems.

Presented in Section 2 is a description of MICAP along with some comparisons of calculated results with experimental data. Section 3 contains the analysis of hydrogen knock-in utilizing the MICAP system.

2. MICAP: THE CODE AND COMPARISON WITH EXPERIMENTAL DATA

2.1 The Code System

This Monte Carlo code utilizes all partial cross sections, angular distributions, and secondary energy distributions currently available in the Evaluated Nuclear Data File, ENDF/B-V as required for the Monte Carlo random walk procedure. The data formats and procedures for processing the ENDF/B-V nuclear data are presented in Ref. 10. The recommended procedures are followed explicitly in the neutron cross section processors to assimilate the data into a format suitable for Monte Carlo analysis. In general, this involves formatting the cross sections into linearly interpolable cross section energy pairs, formulating the angular distributions into normalized energy-dependent cumulative distribution functions, and formulating the secondary energy data into either tabulated probability distribution tables or into a data format suitable for sampling with one of the ENDF/B-V secondary energy distribution functions (Watt spectrum, evaporation spectrum, etc.).

All of the nuclear data in ENDF/B-V are tabulated for the laboratory reference system except the neutron elastic and discrete inelastic scattering angular distributions. These data are tabulated for the center-of-mass reference system because these neutron interactions are isotropic in the center-of-mass system for a wide range of neutron energies. Since the Monte Carlo random walk occurs in the laboratory system, exact angle-energy relationships derived from basic energy/momentum principles are used to calculate the emergent neutron energy and direction.

To account for neutron scattering at thermal energies, the free gas model is used since it yields a good approximation to the thermal flux spectrum and can be sampled without tables. The free gas scattering model assumes that the neutrons are transported in a monatomic gas having an isotropic Maxwellian distribution of velocities. To obtain the emergent neutron energy and angle, the three velocity components of the target nucleus

are sampled from the Maxwell-Boltzmann distribution. The emergent neutron direction is sampled from an isotropic distribution in the center-of-mass system. The emergent neutron energy and direction in the laboratory system is then determined through conservation of energy and momentum.

The emergent neutron parameters for all other reactions treated as scattering type reactions are expressed in terms of post-collision energy and direction in the laboratory system. These scattering type reactions include the continuum mode of inelastic scattering, (n,2n), (n,3n), (n,fission), and (n,n'x) where x represents a charged particle (proton, alpha particle, etc.). In these reactions, the emergent neutron angle is selected from an ENDF/B-V tabulated angular distribution and the emergent neutron energy is selected from an ENDF/B-V tabulated probability distribution or from an evaporation spectrum except for the (n,fission) reaction which uses an energy dependent Watt spectrum. Because of the structure of ENDF/B-V data, single neutron emission models are used for the (n,2n), (n,3n), and (n,fission) reactions with the weights of the emergent neutrons multiplied by two, three and $\nu(E)$, respectively. The parameter, $\nu(E)$, is the average number of neutrons produced per fission event tabulated as a function of energy.

All charged particle production via absorption reactions i.e., (n,p), (n,α), (n,d), etc., or inelastic scattering reactions with charged particle emission assume isotropic emission of the charged particle in the laboratory system. The charged particle emergent energy is selected from a general evaporation spectrum which has been modified to account for Coulomb barrier and Q value effects.[5]

All compound nuclei excited through neutron interactions (except elastic scattering) possess the potential of emitting one or more photons while decaying to ground state. Therefore, for every neutron interaction except elastic scattering, a check is made to determine if secondary photon production data are available. If there are data available, a photon is produced with a direction assumed isotropic in the laboratory system, an energy selected from the ENDF/B-V tabulated distribution, and weight equal to the ENDF/B-V energy dependent multiplicity. There are some materials with absorption reactions resulting in ground state transitions. For these reactions a test is implemented to insure no secondary photon generation occurs.

The photon production capability is programmed to model the natural physical processes as accurately as possible. Unfortunately, the photon production data in ENDF/B-V are not well known for some of the individual neutron interactions in many materials. Consequently, for these materials, the ENDF/B-V photon production data have been lumped into one file encompassing the individual neutron interactions which might produce a secondary photon. The neutron transport code utilizes these data to produce a photon whose direction, energy, and weight are representative average values for these neutron interactions.

Each neutron interaction produces at least a recoil heavy ion. In response analysis, recoil heavy ions can deposit energy in the active medium thereby contributing to the detector signal. Therefore, the energy and direction of the recoil heavy ions must be determined for each neutron interaction. This is accomplished using energy and/or momentum balances for all incident and exit particles produced in the collision.

The transport of all gamma rays produced is carried out using a modified EGS/PEGS code system.[11]

In solving the Boltzmann transport equation for charged particles, i.e., protons, alpha particles, recoil heavy ions, etc., the only interactions considered in the present work are "continuous" energy loss mechanisms. Most recoiling ions are low in energy and will range out before interacting. To simulate a Monte Carlo random walk, a very small fictitious transport cross section is incorporated to determine the next "collision" site. Because this cross section is very small (1.0×10^{-10}), the charged particle transport kernel will always provide the distance to the material boundary as the distance to be transported. Prior to transport, the particle's range for complete energy loss is calculated from the stopping power and range/energy table.[12] If the particle's range is less than the distance to the material boundary, all the particle's energy is assumed deposited in the material. If the range is greater than the distance to the material boundary, the stopping power and range/energy table are used to determine the fraction of energy deposited in the material and the particle is transported to the material boundary losing this amount of energy. This process is repeated until the particle loses all of its energy.

Recombination effects are sometimes a problem in gas or liquid ionization chambers. Recombination results from ionized electrons recombining with charged ions thereby decreasing the charge collected. If recombination effects are significant, the nonlinearity of the charge collected (Q) (or light collected as is the case for plastic scintillators) is taken into account using Birks' law.[13]

As with the other general Monte Carlo codes, MICAP is a three-dimensional, multimedia code wich utilizes combinatorial geometry and can therefore model any detector configuration.

2.2. System Verification and Results

Establishing the validity of the MICAP code system involved implementation of a five part verification program. The verification program included comparing results obtained with existing code systems and comparing with experimental results. Each part of the verification program investigated a particular aspect of the radiation transport processes applicable to detector analysis. More specifically, the verification program involved comparisons with the MORSE,[6] MACK-IV,[14] RECOIL,[15] and O5S[16] codes. The comparisons with these codes is excellent.

O5S is a specialized Monte Carlo code for calculating pulse height distributions due to monoenergetic neutrons incident on organic scintillators and is specialized in that the code handles only carbon-hydrogen organic compounds and models only right circular cylinders. No gamma production is considered. O5S is further restricted in the carbon and hydrogen neutron reactions which are allowed to occur. Even with the above restrictions, O5S has been used extensively to calculate pulse height distributions for calibration experiments with monoenergetic neutrons.

The calculations involved modeling a monodirectional 14.2 MeV monoenergetic neutron source distributed over the flat face of a cylindrical polyvinyltoluene (grade BC501) plastic scintillator.

The comparison of the pulse height distributions generated in O5S and MICAP is presented graphically in Fig. 1. Both distributions are normalized to 60,000 contributing source particles and plotted as functions of energy in cobalt units. One cobalt unit is the base-line intercept of a straight line fit to the high end of a ^{60}Co gamma ray pulse height distribution.[16] The comparison in Fig. 1 shows excellent agreement between O5S

and MICAP. Three distinct contributions can be seen in the pulse height distributions presented in Figure 1, with each contribution dominated by a different particle type. The low energy contribution (below 4 x 10^{-2} cobalts) is due primarily to carbon recoil, the intermediate energy contribution (between 4 x 10^{-2} and approximately 8 x 10^{-1} cobalts) is due primarily to alpha particle production, and the high energy contribution (above approximately 8 x 10^{-1} cobalts) is due primarily to proton recoil. The carbon recoil and proton recoil pulse heights agree to within the statistics of the Monte Carlo calculations. The alpha particle recoil pulse heights, however, reflect differences in the models employed in the two programs.

The two neutron reactions generating the alpha particle recoil pulse

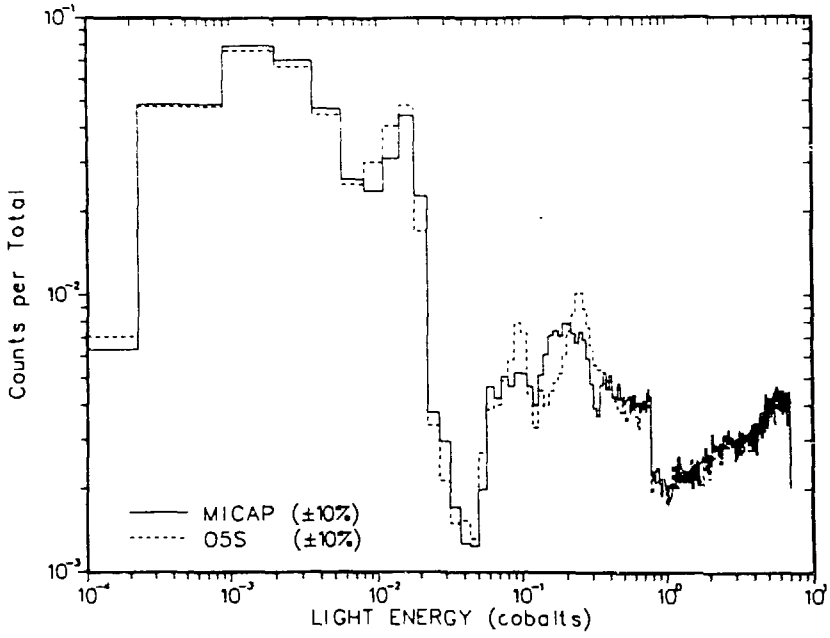

Fig. 1. Comparison of MICAP and 05S pulse height distributions for a BC501 polyvinyltoluene plastic scintillator with a monodirectional 14.2 neutron source.

height are the $^{12}C(n,n'3\alpha)$ and the $^{12}C(n,\alpha)$ reactions. In viewing Fig. 1, the pulse height for 05S contains two distinct peaks at approximately 1.0 x

10^{-1} and 2.5 x 10^{-1} cobalts and a small peak at approximately 7.5 x 10^{-1} cobalts. The two large peaks are produced by alpha particles generated from the $^{12}C(n,n'3\alpha)$ reaction and the small peak is produced by alpha particles generated from the $^{12}C(n,\alpha)$ reaction. The two large distinct peaks result from the O5S treatment of $^{12}C(n,n'3\alpha)$ collisions. Carbon contains eighteen discrete levels of inelastic scattering capable of decaying to ground state via three alpha particle emission. To simplify programming and save core storage space, O5S allows only the three most probable levels to occur. Two of these levels occur 95% of the time (in O5S) and correspond to the two distinct peaks shown in Fig. 1. MICAP maintains all discrete levels of inelastic scattering data and therefore generates much broader peaks in the alpha particle pulse height distribution. The MICAP pulse height distribution is considered a more accurate representation of the true pulse height distribution. While the spectral shapes in the alpha particle pulse height are different, the integral contributions are in excellent agreement.

Additional comparisons between O5S and MICAP were made on the zero bias efficiency (defined as the number of source particles undergoing at least one collision divided by the total number of source particles) and on the average number of collisions per colliding neutron. O5S calculated a zero bias efficiency of 0.37 and 1.41 collisions/colliding neutron. The MICAP results were in excellent agreement with a zero bias efficiency of 0.36 and 1.46 collisions/colliding neutron.

To demonstrate the ability of MICAP to calculate ionization chamber response functions, several monoenergetic photon calibration experiments were analyzed. One experiment, calculated and described in this report, was the Health and Safety Laboratory (HASL) calibration experiment of the high pressure argon spherical ionization chamber systems used in the measurement of environmental radiation exposure rates.[17] The comparison of the MICAP and experimental results are shown in Table 1 for the HASL calibration experiments. As seen in Table 1, the calculated-to-experimental ratios (C/E) show excellent agreement for almost all cases. The calculations agreed to within 10% of the experimental values in all but two cases. These are absolute comparisons based on gamma source yields.

To demonstrate the ability of MICAP to calculate detector response functions for mixed neutron and photon radiation environments, three radiation experiments were analyzed.[18,19] The first experiment analyzed was performed at the NBS ^{252}Cf facility. This experiment involved exposing the 50 cm^3 and 0.5 cm^3 ionization chambers individually, in free air, at a nominal distance of 30 cm from the center of the ^{252}Cf source. The second and third experiments were performed at the AFRRI TRIGA reactor. These experiments were performed in exposure room 1 (ER1) of the reactor facility for two of the most frequently used reactor configurations:

1. Bare room with no shielding placed between the experiment and the reactor core (ER1 Free Field), and
2. 15 cm lead shield placed in front of the reactor tank wall to attenuate photons (ER1 15 cm Pb).

Table 1. Comparison of Measured and Calculated Detector Responses for the Photon Calibration Experiments of the Health and Safety Laboratory (HASL) High Pressure Argon Ionization Chamber

Photon Source	Source Energy (MeV)	Detector Pressure (Atm)	Calculated[b] Response ($A/\mu R\text{-}hr^{-1}$ ($\times 10^{-15}$))	Measured[a] Response ($A/\mu R\text{-}hr^{-1}$ ($\times 10^{-15}$))	C/E
^{241}Am	0.06	9.2	20.2	20.3	0.995
^{141}Cs	0.145	9.2	6.63	7.86	0.844
^{137}Cs	0.662	9.2	3.86	4.03	0.958
^{60}Co	1.25	9.2	3.89	4.00	0.973
^{241}Am	0.06	21.7	20.3	21.9	0.928
^{141}Cs	0.145	21.7	14.1	15.4	0.916
^{137}Cs	0.662	21.7	8.57	8.78	0.976
^{60}Co	1.25	21.7	8.85	9.46	0.936
^{241}Am	0.06	36.8	4.05	4.92	0.823
^{141}Cs	0.145	36.8	18.1	19.3	0.938
^{137}Cs	0.662	36.8	12.3	12.8	0.961
^{60}Co	1.25	36.8	13.1	13.2	0.992

[a] Experimental uncertainty
4% for ^{60}Co source
5% for ^{141}Cs and ^{137}Cs sources
7% for ^{241}Am source

[b] Monte Carlo accuracy (1 standard deviation)
3% for all calculations

The AFRRI experiments exposed a pair of ionization chambers about 10 cm apart and approximately 100 cm from the reactor core center. The two ionization chambers exposed were the 0.5 cm^3 Tissue Equivalent plastic Tissue Equivalent gas (TE/TE) ionization chambers and the 0.5 cm^3 Mg/Ar ionization chamber.

The ionizat[illegible] chambers were modeled exactly using combinatorial geometry. The ma[illegible]als and geometry for the 50 cm^3 AFRRI chambers are shown in Fig. 2 and demonstrate the details included in the calculations.

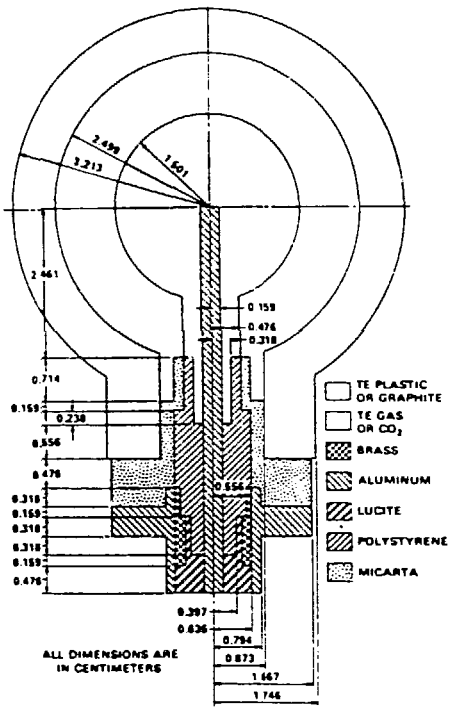

Fig. 2. Geometry configuration for the Armed Forces Radiobiology Research Institute (AFRRI) 50 cm^3 ionization chamber.

Comparisons of the calculated and experimental total ionization chamber responses to the mixed field experiments are presented in Table 2. The calculated-to-experimental ratios (C/E) show excellent agreement in all the cases except the 0.5 cm^3 Mg/Ar chamber in the ER1 15 cm Pb field. Like the monoenergetic photon results, the largest discrepancy (excluding the case mentioned above) occurs for the smallest measured response. A portion of this discrepancy could therefore be due to experimental error. The Monte Carlo results have a fractional standard deviation less than ±10% for all calculations. To compare with the measured response, an absolute normalization was obtained from the spectra presented in Ref. 20 for the

two AFRRI experiments. While the spectral shapes in Ref. 20 are probably accura to within ±10%, the absolute normalization is known to within only ±15-20%, especially for the AFRRI ER1 15 cm Pb cases. Therefore, in most cases, the MICAP calculated results in Table 2 are within the statistical error of the information used.

Table 2. Comparison of Measured and Calculated Detector Responses for the Mixed Neutron and Photon Radiation Field Experiments of the Armed Forces Radiobiology Research Institute (AFRRI) Ionization Chambers

Radiation Field	Detector Volume (cm^3)	Detector Type	Calculated Response (pA)	Measured[a] Response (pA)	C/E
^{252}Cf	50	C/CO_2	6.51 (0.023)[b]	7.21	0.903
^{252}Cf	50	TE/TE	12.2 (0.062)	12.4	0.984
^{252}Cf	0.5	Mg/Ar	0.061 (0.019)	0.078	0.782
^{252}Cf	0.5	TE/TE	0.105 (0.012)	0.130	0.808
ER1 FF	0.5	Mg/Ar	7.10 (0.037)	6.42	1.11
ER1 FF	0.5	TE/TE	8.21 (0.021)	7.70	1.07
ER1 15cm Pb	0.5	Mg/Ar	4.42 (0.072)	7.16	0.617
ER1 15cm Pb	0.5	TE/TE	8.66 (0.007)	8.75	0.990

[a]Experimental uncertainty ± 5%.

[b]Fractional standard deviation ($\sigma(\bar{x})/\bar{x}$).

The AFRRI ER1 15 cm Pb calculation using the 0.5 cm^3 Mg/Ar ionization chamber displayed an interesting result in the neutron response analysis. In this detector, a thin polyethylene strip (approximately 0.1-cm-high) is in contact with the gas region. The polyethylene acts as an insulator between the outside wall and the central electrode. The analysis of the results shows recoil argon ions from neutron interactions in the gas, and proton recoils from neutron interactions with hydrogen in the polyethylene

strip (hydrogen knock-in), as the only two sources of energy deposition in the gas. Furthermore, approximately 80% of the total signal (due to neutrons) originates from the proton knock-ins from the polyethylene strip. This result is significant in that undersampling has probably occurred in the MICAP results for the polyethylene strip in the 0.5 cm^3 Mg/Ar chamber if the experimental results are correct, the geometry is correct, and the source is correct and reasonably gamma free. Because the photon component of the total signal is dominant in the ^{252}Cf and in the AFRRI ER1 FF results, the undersampling would not cause a large discrepancy in a comparison of calculated and experimental total responses for these radiation fields. The AFRRI ER1 15 cm Pb field is predominantly a neutron field however, and the 0.5 cm^3 Mg/Ar ionization chamber is designed to be highly neutron insensitive. A method which would make this detector even more neutron insensitive would be to replace the polyethylene with a non-hydrogeneous insulating material. This would mitigate the proton recoil component of the neutron signal and make the 0.5 cm^3 Mg/Ar chamber truly neutron insensitive.

3. HYDROGEN KNOCK-IN

The geometry, materials, and sources considered in the hydrogen knock-in calculations are presented in Fig. 3. Some of the results obtained are presented in Tables 3 and 4. As can be seen in Table 3, substantial increase in total deposited energy can be expected due to hydrogen knock-in. By considering a ^{238}U fission spectrum, which crudely represents the neutron spectrum in a calorimeter, a 41% increase can be expected. Several calculations were carried out varying the plastic thickness so that an optimum thickness could be obtained. These results indicated that 100 to 200 microns produce the optimum thickness with respect to energy knocked-in.

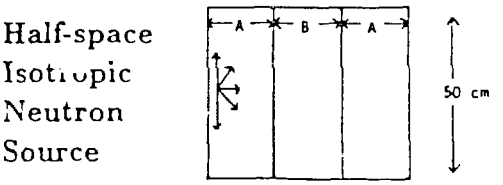

A = plastic, $CH_{1.2}$, $\rho = 1.04\ g/cm^3$

0.0, 0.0025, 0.0050, 0.010, 0.020, and 0.040 *cm*

B = Silicon, $\rho = 2.35\ g/cm^3$

0.01, 0.02, and 0.04 *cm*

Sources considered

a) U^{238} fission spectrum

b) Mono-energetic neutrons of energy

15, 12, 10, 7, 5, 2, and 1 MeV

Fig. 3. Geometry, sources, and materials used in the calculations.

Table 3. Energy Deposition in Silicon Due to Neutrons of Various Energies

Neutron Source Energy (MeV)	Total Energy Deposited in Si (MeV)	Energy Deposited in Si by H Knock-in (MeV)	Energy Deposited in Si by Coll in Si (MeV)	% Increase in Energy Deposited
15.	4.70-2[b]	1.29-2	3.41-2(3.57-2)[c]	37.8%
12.	4.08-2	1.14-2	2.94-2(3.06-2)	38.8%
10.	3.65-2	1.10-2	2.55-2(2.62-2)	43.1%
7.	2.48-2	8.17-3	1.66-2(1.70-2)	49.4%
5.	9.55-3	4.31-3	5.24-3	82.3%
2.	2.48-3	6.41-4	1.84-3	34.8%
1.	1.65-3	1.30-4	1.52-3	8.6%
^{238}U fission spectrum	4.02-3	1.16-3	2.86-3	41.0%

[a] 0.01-cm plastic, 0.04-cm Si, data normalized per source neutron.
[b] Read as 4.70×10^{-2}.
[c] Energy deposited in Si by collisions in silicon without ion transport.

Presented in Table 4 are data that indicated that the energy deposited in the silicon by hydrogen knock-in may occur rather sporadically and introduce larger fluctuation leading to a larger resolution or a non-Gaussian pulse height distribution warped to the high energy side. As can be seen, the collision efficiency of the neutrons with the silicon is small. However, the hydrogen knock-in efficiency is even smaller, about 10 to 20 times. It has been demonstrated in the previous table that the total knock-in energy and total energy deposited by direct collisions can be approximately the same, therefore, single event knock-in energy when it occurs must be approximately 10 times larger. This may introduce larger fluctuations due to sporadic dumps of large energy. As can be seen for the fission spectrum, 34.7 silicon collisions must occur before 1 knock-in occurs.

Table 4. Knock-In Efficiency and Average Energy Knocked-In as a Function of Neutron Energy

Neutron Energy (MeV)	Coll Eff in Si (%)	H Knock-in Eff % (MeV)	Avg Energy Deposited per Coll in Si (MeV)	Avg H Energy Deposited per H Knock-in Coll (MeV)	Coll Eff in Si per Knock-in Eff
15.	1.99	0.183(0.451)[b]	1.71	7.05	10.9
12.	2.03	0.199(0.542)	1.45	5.73	10.2
10.	1.98	0.224(0.654)	1.29	4.91	8.84
7.	1.99	0.247(0.883)	0.834	3.31	8.06
5.	2.44	0.210(1.07)	0.215	2.05	11.6
2.	2.59	0.0820(1.85)	0.0710	0 782	31.6
1.	3.97	0.0356(2.50)	0.0383	0.365	112.
^{238}U fission spectrum	2.18	0.0810(2.25)	0.102	1.43	34.7

[a] 0.01-cm plastic, 0.04-cm Si, data normalized per source neutron.
[b] Collision efficiency in the plastic.

Using the data generated, it can be shown that for a 3 GeV π^- incident on a uranium/silicon calorimeter, hydrogen knock-in occurs only 50% of the time or 1 knock-in/6 GeV of incident energy. This result has been

confirmed by a more detailed calculation using MICAP in conjunction with CALOR. If the total energy in jets are measured in a calorimeter, then the fluctuations associated with hydrogen knock-in will be reduced. For example, a 100 GeV jet will produce on the average 16.7 knock-ins with a σ of approximately 4 and this 25% fluctuation in the knock-in energy translates to a few percent fluctuation in the total energy deposition. Therefore, using hydrogen knock-in for low-energy calorimetry does not appear promising. However, it may be useful at higher energies. At higher energies, the jet resolution improves as the e/h ratio approaches 1.[21]

Presented in Table 5 are preliminary results of 3 GeV π^- incident on a uranium/silicon calorimeter. The data in the base case were obtained using CALOR with MORSE or with MICAP. For this particular calculation, the MORSE results represent an average of two extreme methods for calculating the energy deposition. It is somewhat fortuitous that MORSE and MICAP gave exactly the same answer. As can be seen, the e/h ratio is larger than 1. The modified cases for the most part have been obtained by using the data generated by MICAP using the ^{238}U fission spectrum as the source. As the data indicate, the e/h ratio can be made ≈ 1 if a smaller thickness of silicon is used, i.e., 100 microns. This thickness may be achieved by partially depleting thicker devices.[22] The data in this table are still very preliminary, and more detailed analysis is warranted before absolutely final conclusions can be reached.

Table 5. Very Preliminary Results for 3 GeV π^- Incident on a Uranium/Silicon Calorimeter

(MeV)	Base Case[a] Shown Data (MeV)	Modified Cases Based on[b] A	B
Primary Protons, secondary Protons and pions, heavy ions and muons.	12.04	12.04	3.01
Neutral pions and de-excitation and fission gamma rays from all charged particles and neutrons with energy > 20 MeV.	3.16	3.16	0.79
Low energy neutrons (E < 20 MeV).	1.70(1.70)[c]	2.39(3.15)[c]	1.27
De-excitation and fission gamma rays from low energy neutron collisions.	0.55	0.55	0.14
	17.45	18.14(18.90)	5.21
e/h	1.33	1.28(1.23)	1.11

[a]0.5 cm U, 0.13 cm air gap, 0.10 cm G-10, 0.04 cm Si, 0.10 cm G-10, 0.13 cm air gap repeated 130 times, width 50 x 50 cm^2.

[b]A: 0.5 cm U, 0.13 cm air gap, 0.10 Plastic, 0.04 cm Si, 0.10 cm Plastic, 0.13 cm air gap.
B: 0.5 cm U, 0.145 cm air gap, 0.10 cm Plastic, 0.01 cm Si, 0.10 cm Plastic, 0.145 cm air gap.
Data obtained from the Base Case and data in previous tables for the low energy neutrons and the assumption that the signals scale linearly with Silicon thickness.

[c]Obtained from MICAP in conjunction with HETC.

4. REFERENCES

1. A. Nakamoto et al., Nucl. Instrum. Methods A251, 275 (1986).
   T. Akesson et al., CERN/EP87/88, May 12, 1987.

2. C. W. Fabjan et al., Phys. Letts. 60B, 105 (1975); Nucl. Instrum. & Methods A238, 489 (1985).

3. J. Brau and T. A. Gabriel, Nucl. Instrum. & Methods A238, 489 (1985).

4. H. Bruckmann et al., DESY 87-064 (June, 1987).

5. J. O. Johnson and T. A. Gabriel, Oak Ridge National Laboratory Report

ORNL/TM-10196 (1987).

6. M. B. Emmett, Oak Ridge National Laboratory Report ORNL-4972 (1975).

7. Los Alamos Radiation Transport Group X-6, Los Alamos National Laboratory Report LA-7396-M (Revised April 1981).

8. J. C. Nimal et al., TRIPOLI-2, C.E.A., Saclay, France (1980).

9. T. A. Gabriel et al., "CALOR87: HETC87, MICAP, EGS4, and SPECT, A Code System for Analyzing Detectors for Use in High Energy Physics Experments," Proceedings of the Workshop on Detector Simulation for the SSC, Argonne National Laboratory, August 24-28, 1987.

10. R. Kinsey, BNL-NCS-50496, Brookhaven National Laboratory (1979).

11. R. L. Ford and W. R. Nelson, SLAC-210, Stanford Linear Accelerator Center, 1978. (EGS4 is now incorporated into MICAP and CALOR.)

12. T. W. Armstrong and K. C. Chandler, Oak Ridge National Laboratory Report ORNL-4869 (1973).

13. J. B. Birks, *The Theory and Practice of Scintillation Counting*, The Macmillian Company, New York (1964).

14. M. A. Abdou et al., Argonne National Laboratory Report ANL/FPP/TM-77-5 (1978).

15. T. A. Gabriel et al., Oak Ridge National Laboratory Report ORNL/TM-5160 (1976).

16. R. E. Textor and V. V. Verbinski, Oak Ridge National Laboratory Report ORNL-4160 (1968).

17. J. A. DeCampo et al., Health and Safety Laboratory Report HASL-260, New York (1972).

18. D. E. Eagleson, Armed Forces Radiobiology Research Institute (AFRRI), Bethesda, Maryland, private communications to J. O. Johnson, Oak Ridge National Laboratory, May-July 1986.

19. 1Lt M. A. Dooley et al., TR-86-3, Armed Forces Radiobiology Research Institute (1986).

20. V. V. Verbinski and C. G. Cassapakis, Defense Nuclear Agency, DNA 5793F-2, Washington, D.C. (1981).

21. T. Akesson et al., Nucl. Instrum. & Methods A241, 17 (1985).

22. G. Barbiellini et al., Nucl. Instrum. & Methods A240, 289 (1985).